

DETC2011-4, \$&+

## FINITE ELEMENT MODELING OF A MICRODROPLET GENERATOR WITH INTEGRATED SENSING

**William S. Rone**

Robotics and Mechatronics Laboratory  
The George Washington University  
Washington, DC, USA

**Pinhas Ben-Tzvi\***

Robotics and Mechatronics Laboratory  
The George Washington University  
Washington, DC, USA

### ABSTRACT

This paper describes the analysis of a novel microdroplet generator's integrated sensing capability using finite element simulation. The dominant paradigm for utilizing droplet generation is with either open-loop or externally-sensed closed-loop methods, each with significant disadvantages in terms of reliability and large-scale implementation, respectively. This work utilizes a system designed with a compressible gas reservoir adjacent to the incompressible droplet liquid reservoir. The compressible gas pressure changes as liquid droplets are dispensed from the constant volume fluid reservoir. This change was found to be linearly dependent on the size of the droplet that was ejected, validating this gas reservoir pressure as a useful means of indirectly measuring droplet size internally within the system.

### KEYWORDS

MEMS, microfluidics, droplet generation, finite element analysis, COMSOL, multiphysics simulations

### NOMENCLATURE

|                    |  |
|--------------------|--|
| $F$                | External force (N)                     |
| $F_{fr}$           | Frictional force (N)                   |
| $g$                | Gravity vector ( $m/s^2$ )             |
| $n$                | Normal vector (unitless)               |
| $p$                | Pressure (Pa)                          |
| $u$                | Velocity vector, $[u \ v \ w]^T$ (m/s) |
| $\beta$            | Slip length (m)                        |
| $\gamma$           | Reinitialization parameters (unitless) |
| $\varepsilon_{IS}$ | Interface thickness parameter (m)      |
| $\theta_w$         | Contact angle (rad)                    |
| $\mu$              | Absolute viscosity (Pa·s)              |
| $\rho$             | Density ( $kg/m^3$ )                   |
| $\phi$             | Level set variable (unitless)          |

### INTRODUCTION AND BACKGROUND

As microdroplet generators have developed from novel concepts to critical laboratory instruments, two key considerations have dominated their development: the reduction of droplet size and the implementation of novel actuation mechanisms. However, device-based integrated sensing of droplet generation has seen minimal study.

As researchers have pushed droplet diameters to the micrometer range and developed innovated actuation mechanisms for generating droplets, a new focus on designing integrated systems capable of robust feedback control is the next frontier for developing precision lab automation devices capable of sub-picoliter droplet dispensing. The first step in developing this type of system is twofold: determining a sensible property to allow the size of a generated droplet to be monitored by the control system and choosing an actuation mechanism with easily controllable parameters for real-time adjustment.

### Current Actuation Mechanisms

Piezoelectric and thermal actuation mechanisms dominate the approach used in commercial generators, though several other novel actuation concepts have been developed. For a detailed assessment of the field of microdroplet generation, including these other techniques, see [1].

Piezoelectric actuators utilize the inverse piezoelectric effect to convert a potential difference applied across the actuator into a mechanical force. Piezo-actuators can operate in four modes: (i) push-mode, where the piezo imparts a linear motion to generate a droplet [2]; (ii) squeeze-mode, where the piezo expands and contracts to generate a droplet [3]; (iii) bend-mode, where the piezo bends due to constraints at its boundaries preventing it from displacing linearly to generate droplets [4]; and (iv) shear-mode, where the piezo's boundaries are further constrained to exhibit shear deflection under application of a voltage to generate droplets [5].

Thermal actuators utilize thermal energy to create droplets. Three types of thermal actuators have been studied: (i) thermal bubble, where a heater is used to locally form a gas bubble in the liquid reservoir to force a droplet out of the nozzle [6]; (ii) thermal spark, where a spark between two wires or lasers is used to rapidly create a bubble to actuate generation [7]; and (iii) thermal bulking, where thermal expansion of a portion of the generator assembly is used to actuate generation [8].

### Current Sensing Tools

External instrumentation is the most common method for monitoring the occurrence of droplet generation and droplet volume. The most common is photography, where droplet volume is determined by assuming axisymmetry of droplets and processing planar images to calculate volume [4,7]. Dispensed volume weight measurement utilizes a microbalance to weigh droplets as they are produced, accounting for evaporation that may occur, and correlating that weight to the droplets' volumes [9].

Integrated sensing has been less common in generator system design, where the measured data could be used by the device for real-time control and/or passed on to the system's operator. Optical sensors have been used to monitor the occurrence of generation [10], and capacitive sensors have been used to measure fluid pressure and piezo displacement for clogging monitoring and piezo hysteresis compensation [11].

### Current and Future Applications

In biological and chemical synthesis and analysis, one promising application of microdroplet generation is DNA and protein microarray generation, where generators either deposit previously synthesized DNA or proteins on a substrate or synthesize DNA *in situ* on the substrate itself [10,12]. Other applications include sample preparation for mass spectrometry [9,13], and solid support creation and modification [12].

In medicine, both therapeutic and regenerative fields include applications of droplet generation. In therapeutics, drug delivery/therapy both orally [12] and transdermally [14] rely on droplet generation to directly create droplets for inhalation/injection or to indirectly create solid capsules for controlled drug release. In terms of regenerative medicine, tissue engineering utilizes generators to dispense biopolymers and cells to form three-dimensional structures and to use growth factors to create vascular structures.

In manufacturing, droplet generation has been utilized in surface coating [15,16], electrical component manufacturing [15,17] and net form manufacturing [18,19].

### DESIGN CONCEPT

Fundamentally, the design concept requires that two different fluids – an incompressible liquid and a compressible gas – be stored in a single fluid chamber. As an actuator creates and ejects a droplet from the liquid reservoir, the gas's volume and pressure will change (beyond the pressure change already occurring within the fluid chamber). This gas pressure change can be related analytically to the volume of the droplet

dispensed, and the analytical calculation can be verified computationally through simulations and empirically by external instrumentation, such as photography or weight measurement.

Figure 1 illustrates a potential implementation of this design concept. A capillary is used as the fluid chamber, and a squeeze-mode piezo actuates generation. One end of the capillary incorporates a flow focusing region and nozzle where generation/ejection of the droplet occurs. The opposite end incorporates a flexible cap that seals the gas reservoir. During actuation, the piezo will contract and expand, deforming the capillary and creating/ejecting a droplet at the nozzle. During ejection, the volume of the reservoir liquid will change, causing a pressure change in the compressible gas reservoir. This gas pressure change will deform the flexible cap, which can be measured by a sensor (e.g. piezoelectric or capacitive) integrated with the cap. The gas inlet/outlet is used to initially aspirate the device, and to modify the gas reservoir pressure if necessary. This design is an extension our previous work [20] with several improvements to facilitate its physical realization on the microscale.

### FINITE ELEMENT MODEL

COMSOL Multiphysics [21] was used to model this design concept manifestation, with two simplifying assumptions. First, the boundary of the flow focusing region was made a line instead of a curve to reduce the mesh density required to

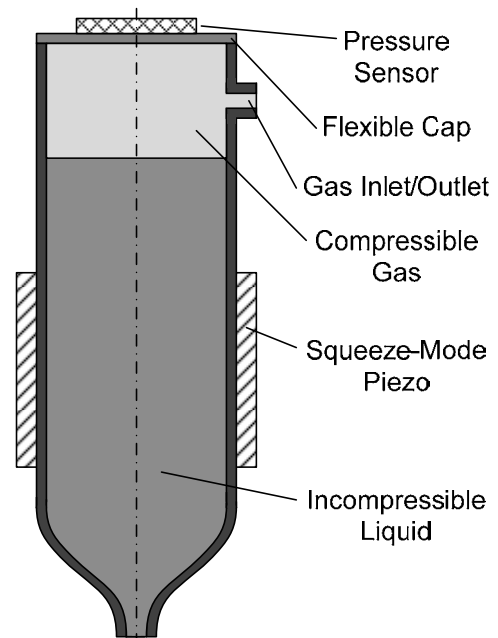


FIGURE 1. SYSTEM DESIGN CONCEPT

accurately represent the system. Second, a pressure boundary condition was used instead of fluid-structure interaction (FSI) to actuate the mode. This simplified the calculation without significant loss of realism because the primary purpose of the squeeze-mode actuator is to eject a droplet by successive positive and negative pressure pulses created in the chamber.

### Geometry

A 2D axisymmetric model was chosen to represent the system. Because squeeze-mode piezoceramic actuation operates in the radial and longitudinal directions and not the tangential, the fluid motion has no impetus to circulate around the axis of symmetry. This assumption simplifies the simulation without loss of utility or accuracy. Figure 2 shows the geometry generated in COMSOL to implement the design concept, with the axis of symmetry coinciding with the lower boundary.

The 50 μm dimension for the nozzle was the primary constraint on the size of the system. This size was chosen based on the average droplet size of another squeeze-mode piezo based generator in [3].

Two points and one segment (a, b & c) are also defined within the geometry: point (a) helps define the wetted wall condition below the fluid interface; point (b) helps define the pressure boundary condition; and segment (c) facilitates a higher mesh density directly downstream of the nozzle.

### Subdomain Properties

The COMSOL Material Library was used to model the liquid and gas in the generator, with water chosen as the liquid and air chosen as the gas. In each model, pressure and temperature were used to define the fluids' density and viscosity. T = 25°C was used as the temperature input, while the pressure input was coupled to the pressure variable  $p$ .

**Governing Equations.** The four dependent variables needed in this model are a velocity vector field  $\mathbf{u}$  and a scalar pressure field  $p$ . The Cartesian values associated with this

model are converted into cylindrical form by COMSOL, with tangential terms ignored. The governing equations for fluid conservation of mass and momentum, shown as equations (1) and (2), are used to calculate the  $\mathbf{u}$  and  $p$  fields.

$$\frac{\partial \rho}{\partial t} + \rho \nabla \cdot \mathbf{u} = 0 \quad (1)$$

$$\rho \frac{\partial \mathbf{u}}{\partial t} + \rho (\mathbf{u} \cdot \nabla) \mathbf{u} = \nabla \cdot \left[ -p \mathbf{I} + \mu (\nabla \mathbf{u} + (\nabla \mathbf{u})^T) - \frac{2}{3} \mu (\nabla \cdot \mathbf{u}) \mathbf{I} \right] + \rho \mathbf{g} + \mathbf{F} \quad (2)$$

**Interface Tracking.** The level set method is used to track the interface of the two fluids by storing the relative composition of the fluid in  $\phi$  that ranges from 0 to 1 ( $\phi = 0$ : 100% gas;  $\phi = 1$ : 100% liquid). Material properties are determined through a weighted combination of the liquid and gas properties. The level set variable conservation equation is shown in (3). The left hand terms account for the conservation of the level set variable. The right hand terms provide numerical stability.

$$\frac{\partial \phi}{\partial t} + \nabla \cdot (\mathbf{u} \phi) = \gamma \nabla \cdot \left( \epsilon_{ls} \nabla \phi - \phi (1 - \phi) \frac{\nabla \phi}{|\nabla \phi|} \right) \quad (3)$$

As an initial condition, each subdomain in the model geometry is assigned to have either  $\phi = \{0,1\}$ , as shown in Figure 2. However, before the mass and momentum equations can be coupled with equation (3), the level set field variable must be made continuous over the fluid interfaces. This is done by solving (3) without the velocity term up to the time  $t \approx 5 \epsilon_{ls} / \gamma$  (as recommended by COMSOL).

### Boundary Conditions

Figure 3 shows and labels the boundaries associated with the model geometry. The labels are defined in Table 1. At each unlabeled internal boundary, a continuity condition is applied.

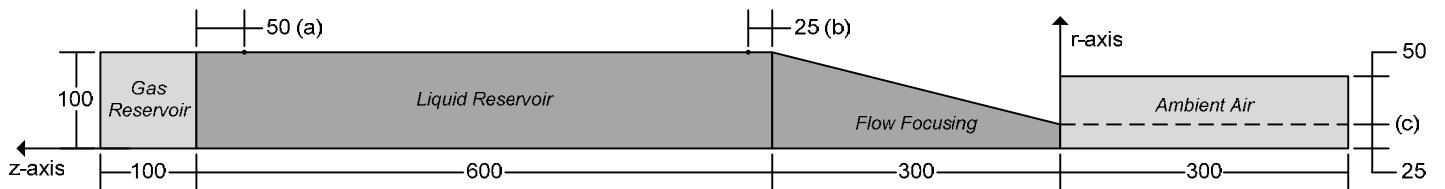


**FIGURE 2. MODEL GEOMETRY AND INITIAL FLUID DISTRIBUTION (DIMENSIONS IN MICROMETERS; DARK SHADING – LIQUID:  $\phi = 1$ , LIGHT SHADING – GAS:  $\phi = 0$ )**

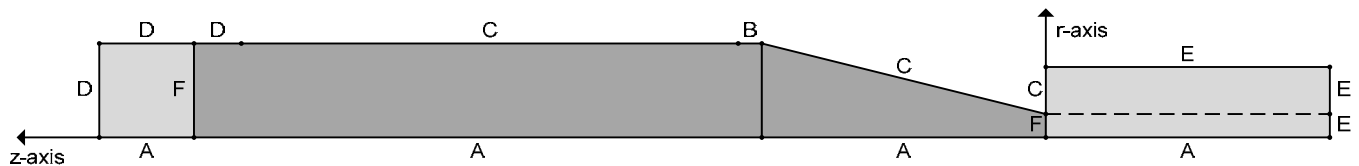


**FIGURE 3. MODEL BOUNDARIES**

**TABLE 1. BOUNDARY TYPES**

| Label | Boundary Type                           | Equations   |
|-------|---|---|
| A     | Symmetry – Axial                        | $u_r = 0$   |
| B     | Inlet – Pressure,<br>No Viscous Stress  | $p = \text{pressure}$<br>$[\mu(\nabla\mathbf{u} + (\nabla\mathbf{u})^T)]\mathbf{n} = 0$<br>$\phi = 0$ |
| C     | Wall – No-Slip                          | $\mathbf{u} = \mathbf{0}$   |
| D     | Wall – Wetted                           | $\mathbf{n} \cdot \mathbf{u} = 0$<br>$\mathbf{F}_{fr} = -\frac{\mu}{\beta}\mathbf{u}$                 |
| E     | Outlet – Pressure,<br>No Viscous Stress | $p = 0$<br>$[\mu(\nabla\mathbf{u} + (\nabla\mathbf{u})^T)]\mathbf{n} = 0$                             |
| F     | Initial Interface                       | $\phi_0 = 0.5$  |

The time dependent waveform  $P(t)$  for pressure actuation can be extrapolated from an understanding of how the squeeze mode piezo actuates the system. As shown in Figure 4(a), in its simplest operation, the piezo contracts around the capillary, then releases, creating sequential positive and negative pressure pulses, as shown in Figure 4(b). The magnitude of this pulse is taken as a variable input, and the period as  $8 \mu\text{s}$ .

A wetted wall is utilized at locations where the fluid interface is expected to move along the wall. Two parameters define this condition: slip length  $\beta$ , which is coupled to mesh size, and contact angle  $\theta_w$ , which is taken as a constant  $\pi/2$ .

A pressure-based outlet boundary condition is used at two sides of the gas domain downstream of the nozzle to prevent boundary layer effects on the droplet motion.

**Mesh**

A triangular unstructured mesh is used in this model, as shown in Figure 5. The mesh is refined in areas in which a fluid interface is expected to move. Specifically, this is seen within the gas region of the liquid reservoir, and in the gas region downstream of the nozzle where the droplet forms, breaks off and travels away from the nozzle. Furthermore, this specific mesh type was found to be superior to both structured and

unstructured quadrilateral meshes in terms of efficiency and stability.

**SIMULATIONS AND ANALYSIS**

The FEA model described in the previous section was solved for varying input pressure magnitudes. Depending on the applied pressure magnitude, there could be one of two results, as shown in Figure 6. The first result produces no droplet generation, when the pressure magnitude lies below some critical value for the system. A droplet may form at the nozzle, but insufficient inertia exists to overcome the viscous force and surface tension. The second result produces successful droplet generation, when the pressure magnitude exceeds the critical value. This causes a droplet to form at the nozzle during the positive pressure regime, and then continue to move away from the nozzle during negative pressure, causing the droplet to break away from the liquid reservoir.

The critical pressure for transitioning from no generation to successful generation was found to be between 1.2 and 1.3 **MPa**. Based on these results, boundary pressure magnitudes in the range of 10 to 18 **MPa** were simulated and analyzed to explore the behavior of the pressure air gap in both regimes.

Figure 7 shows the gas gap pressure over time for three different actuation pressure magnitudes. The first,  $p_{mag} = 1.0 \text{ MPa}$ , occurs in the no generation regime, while the other two,  $p_{mag} = \{1.3, 1.5\} \text{ MPa}$ , cause ejection. As can be seen, the shape of the gas reservoir pressure in the gap remains approximately the same regardless of actuation magnitude; however, the maximum pressure reached by the gas increases and occurs later in the actuation cycle as the actuation magnitude increases. In each case, it also appears the pressure slowly tapers off beyond the maximum value. Toward the end of the actuation cycle, the pressure boundary condition exerts a low pressure on the liquid reservoir, ending at  $0 \text{ Pa}$  at  $t = 8 \mu\text{s}$  and remaining zero for all future  $t$ . Holding the reservoir at this constant pressure differs from how the system would actually behave, where the direct effects of the actuator on the system would end at the end of the actuation period. But because this consideration occurs after the maximum pressure, it still allows

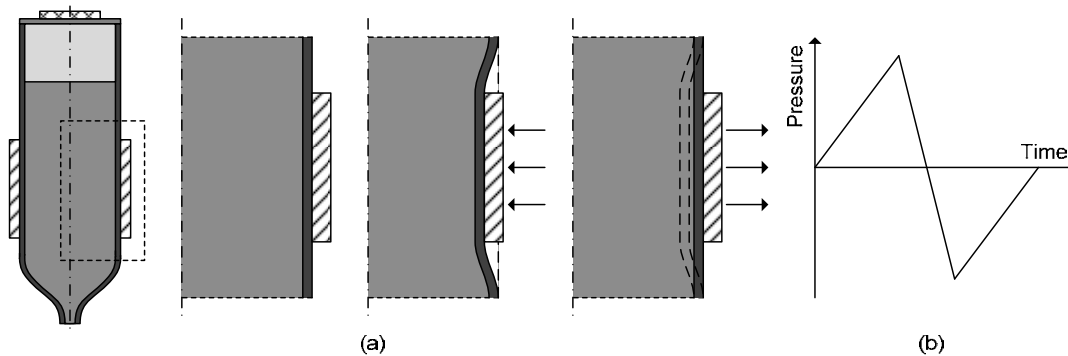


**FIGURE 4. (a) ACTUATION MECHANISM (b) PRESSURE WAVEFORM**

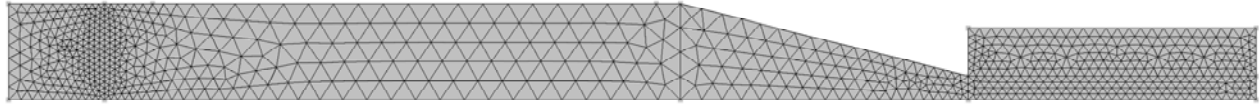


FIGURE 5. MODEL MESH

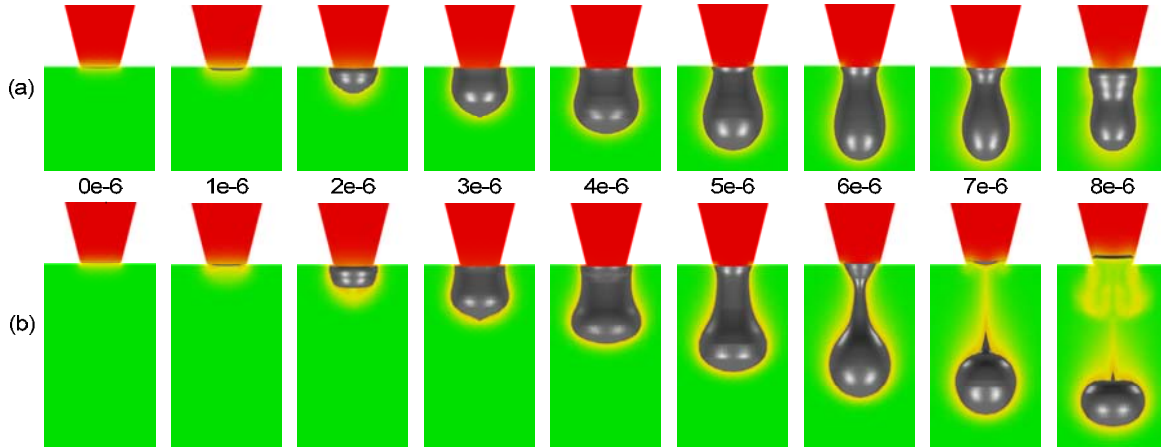


FIGURE 6. SIMULATION VISUALIZATIONS (a) NO GENERATION – PRESSURE MAGNITUDE: 1.0 MPa  
(b) SUCCESSFUL GENERATION – PRESSURE MAGNITUDE: 1.4 MPa

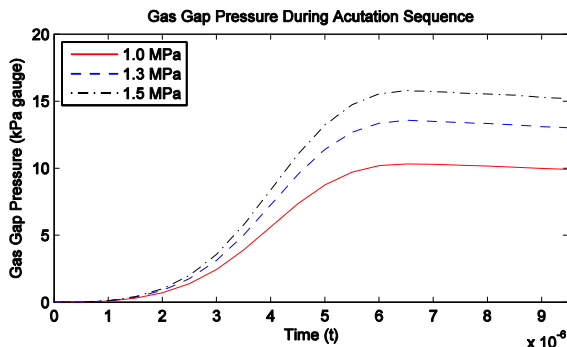


FIGURE 7. GAS RESERVOIR PRESSURE DURING ACTUATION

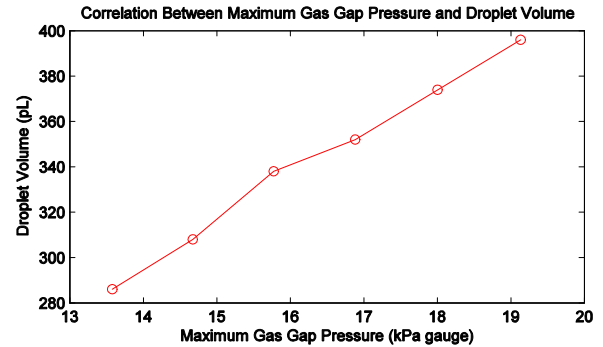


FIGURE 8. DEPENDENCE OF DROPLET VOLUME ON MAXIMUM GAS RESERVOIR PRESSURE

the maximum pressure reached by this gas reservoir to be correlated to the droplet volume produced.

If only actuation pressures that generate droplets are considered, a second metric beyond maximum gas reservoir pressure that can be extracted from the simulations is droplet volume. At each actuation pressure magnitude, these two values can be compared, and have been plotted in Figure 8. As can be seen, a nearly linear correlation can be seen. This linear relationship provides a simple mechanism for indirectly detecting droplet size by measuring the maximum gas reservoir pressure.

## CONCLUSION

The lack of a capacity to produce droplets in closed-loop – measuring their volume in real-time and using that measurement to adjust the dispensing parameters for subsequent generation cycles – is a critical gap in current microfluidic technologies. In this paper, a concept was proposed and tested through simulation for integrating sensing into a droplet generator. This sensing would allow the measurement of the dispensed droplet volume in real-time by monitoring the pressure of a gas trapped in the generator’s fluid reservoir. The FEA simulations performed validated this

correlation between pressure and droplet volume and showed it is linear.

Future work will focus on incorporating fluid-structure interaction and a piezoceramic actuator model in the FEA simulations in order to understand computationally the relationship between the voltage waveform parameters applied to the piezo and the droplet volume and gas gap pressure.

## REFERENCES

- [1] Ben-Tzvi, P. and Rone, W., 2010, "Microdroplet Generation in Gaseous and Liquid Environments," *Microsyst. Technol.*, 16(3), pp. 333-356.
- [2] Ahamed, M.J., Gubarenko, S.I., Ben-Mrad, R. and Sullivan, P., 2010, "A Piezoactuated Droplet-Dispensing Microfluidic Chip," *J. Microelectromech. Syst.*, 19, pp. 110-119.
- [3] Wu, H.C., Lin, H.J. and Hwang, W.S., 2005, "A Numerical Study of the Effect of Operating Parameters on Drop Formation in a Squeeze Mode Inkjet Device," *Model. Simul. Mater. Sci. Eng.*, 13, pp. 17-34.
- [4] Fan, K.C., Chen, J.Y., Wang, C.H. and Pan, W.C., 2008, "Development of a Drop-on-Demand Droplet Generator for One-Drop Fill Technology," *Sens. Actuators A Phys.*, 147, pp. 649-655.
- [5] Brünahl, J. and Grishin, A., 2002, "Piezoelectric Shear Mode Drop-On-Demand Inkjet Actuator," *Sens. Actuators A Phys.*, 101, pp. 371-382.
- [6] Tseng, F.G., Kim, C.J. and Ho, C.M., 2002, "A High-Resolution High Frequency Monolithic Top-Shooting Microinjector Free of Satellite Drops—Part I: Concept, Design and Model," *J. Microelectromech. Syst.*, 11, pp. 427-436.
- [7] Dadvand, A., Khoo, B.C. and Shervani-Tabar, M.T., 2009, "A Collapsing Bubble-Induced Microinjector: an Experimental Study," *Exp. Fluids.*, 46, pp. 419-434.
- [8] Cabal, A., Ross, D.S., Lebens, J.A. and Trauernicht, D.P., 2005, "Thermal Actuator with Optimized Heater for Liquid Drop Ejectors," *Sens. Actuators, A Phys.*, 123-124, pp. 531-539.
- [9] Berggren, W.T., Westphall, M.S. and Smith, L.M., 2002, "Single-pulse Nanoelectrospray Ionization," *Anal. Chem.*, 74, pp. 3443-3448.
- [10] Chang, T.N., Parthasarathy, S., Wang, T., Gandhi, K., Soteropoulos, P., 2006, "Automated Liquid Dispensing Pin for DNA Microarray Applications," *IEEE Trans. Autom. Sci. Eng.*, 3, pp. 187-191.
- [11] Szita, N., Sutter, R., Dual, J. and Buser, R.A., 2001, "A Micropipettor with Integrated Sensors," *Sens. Actuators A Phys.*, 89, pp. 112-118.
- [12] Cooley, P., Wallace, D. and Antohe, B., 2001, "Applications of Ink-Jet Printing Technology to BioMEMS and Microfluidic Systems," *Proc. SPIE Conf. Microfluid. BIOMEMS*, 4560, pp. 177-188.
- [13] Aderogba, S., Meacham, J.M., Degertekin, F.L., Fedorov, A.G. and Fernandez, F., 2005, "Nanoelectrospray Ion Generation for High-Throughput Mass Spectrometry Using a Micromachined Ultrasonic Ejector Array," *Appl. Phys. Lett.*, 86, 203110.
- [14] Stachowiak, J.C., von Muhlen, M.G., Li, T.H., Jalilian, L., Parekh, S.H. and Fletcher, D.A., 2007, "Piezoelectric Control of Needle-Free Transdermal Drug Delivery," *J. Controlled Release*, 124, pp. 88-97.
- [15] De Gans, B.J., Duineveld, P.C. and Schubert, U.S., 2004, "Inkjet Printing of Polymers: State of the Art and Future Developments," *Adv. Mater.*, 16, pp. 203-213.
- [16] Hebner, T.R., Wu, C.C., Marcy, D., Lu, M.H. and Sturm, J.C., 1998, "Ink-jet Printing of Doped Polymers for Organic Light Emitting Devices," *Appl. Phys. Lett.*, 72, pp. 519-521.
- [17] Szczech, J.B., Megaridis, C.M., Gamota, D.R. and Zhang, J., 2002, "Fine-line Conductor Manufacturing Using Drop-on-Demand PZT Printing Technology," *IEEE Trans. Electron. Packag. Manuf.*, 25, pp. 26-33.
- [18] Lee, T.M., Kang, T.G., Yang, J.S., Jo, J.D., Kim, K.Y., Choi, B.O. and Kim, D.S., 2007, "3D Metal Microstructure Fabrication Using a Molten Metal DoD Inkjet System," *Int. Solid-State Sens. Actuators Microsyst. Conf.*, pp. 1637-1640.
- [19] Sui, G. and Leu, M.C., 2003, "Investigation of Layer Thickness and Surface Roughness in Rapid Freeze Prototyping," *ASME J. Manuf. Sci. Eng.*, 125, pp. 556-563.
- [20] Ben-Tzvi, P., Ben Mrad, R. and Goldenberg, A.A., 2007, "A Conceptual Design and FE Analysis of a Piezoceramic Actuated Dispensing System for Microdrops Generation in Microarray Applications," *Mechatron.*, 17, pp. 1-13.
- [21] COMSOL Multiphysics, Version 4.0a, COMSOL, Inc., <http://www.comsol.com>.